Physics – Uspekhi **37**(3) 289 – 302 (1994)

METHODOLOGICAL NOTES PACS numbers: 04.20. + c

The Sagnac experiment with X radiation

V I Vysotskii, V I Vorontsov (deceased), R N Kuz'min,
P A Bezirganyan, A G Rostomyan

Contents

Abstract. The history and physical prerequisites for the realisation of the Sagnac experiment, that is of the 'vortex optical effect' in the frame of a rotating interferometer, are considered. General relativity is used to develop the theory of propagation for electromagnetic waves in a noninertially moving material medium. The theoretical analysis of the peculiarities of the X-ray and gamma-radiation diffractions has been performed within the system of the three-mirror monoblock crystalline interferometer and resonator, while taking into account their rotations. Experimental studies of the X-ray 'vortex optical effect' were performed on a specially designed autonomous X-ray apparatus (commonly used for X-ray interference investigations), which was put on the rotating platform. A series of fluctuation effects (the temperature drift, the field of random deformations, etc.), which keep the Sagnac experiment out of reach of the limiting accuracy, have been revealed and investigated. The experimental data, obtained in the investigation of the 'vortex optical effect', are compared with the results of the theoretical analysis.

1. Introduction

The Sagnac experiment deserves a special place among the classical experiments in optics which have laid the foundations of the theory of relativity and of modern electrodynamics.

V I Vysotskii, V I Vorontsov (deceased) Faculty of Radiophysics, T G Shevchenko Kiev State University, 252601 Kiev 17, Ukraine. Fax (7-044) 269 25 31
R N Kuz'min Faculty of Physics, M V Lomonosov Moscow State University, Leninskie Gory, 119 882 Moscow Tel. (7-095) 939 12 26, Fax (7-095) 957 64 45, E-mail: kuzmin@runar.phys.msu.su
P A Bezirganyan, A G Rostomyan Faculty of Physics, Yerevan State University, ul. Aleko Monukyana, 375049 Yerevan, Armenia

Received 4 June 1993, in revised form 25 November 1993
Uspekhi Fizicheskikh Nauk **164** (3) 309-324 (1994)
Translated by J I Carasso

Its origins typify the wide interest in the 'ether' problem at the beginning of the 20th century, and the setting up of fundamental optical experiments in many countries. The possibility of detecting absolute rotary motion by using electromagnetic effects of the first order (with respect to v/c) was first suggested by Michelson [1] in 1904.

In 1913 Sagnac constructed an apparatus for studying the propagation of light waves in a rotating ring interferometer [2, 3]. These experiments showed that the rotary motion of the apparatus did not result in the dragging and rotation of the 'ether'. During this work Sagnac discovered the 'vortex optical effect', consisting in effect of the rotary motion of the interferometer on the phase characteristics of waves travelling in opposite directions.

Without going into details the essential aspects of this effect can be described by referring to the diagram of Sagnac's apparatus shown in Fig. 1. Radiation from the light source (*1*) (an incandescent lamp) passes through the semitrans-parent plate 2 which produces two mutually coherent waves. These are circulated by the mirrors (*3*) round the perimeter of the interferometer, of area S, in opposite directions. The same half-silvered mirror (*2*) then adds the waves and produces a system of interference bands on a photographic plate. The rotation of the platform (which supports the interferometer) at an angular velocity Ω induces a phase difference

$$\varphi_1 - \varphi_2 = \frac{8\pi S\Omega}{\lambda c} \tag{1.1}$$

between the waves, with an associated shift in the position of the interference bands on the photographic plate (*4*):

$$\delta x = \pm\frac{4S\Omega}{c}\,. \tag{1.2}$$

Plots of $\varphi_1 - \varphi_2$ and of δx were obtained [2, 3] as functions of wavelength λ by the use of the formulae of the special theory of relativity, though the rotating platform was a noninertial system and an exact description of the processes on this platform can be provided only by the general theory of relativity.

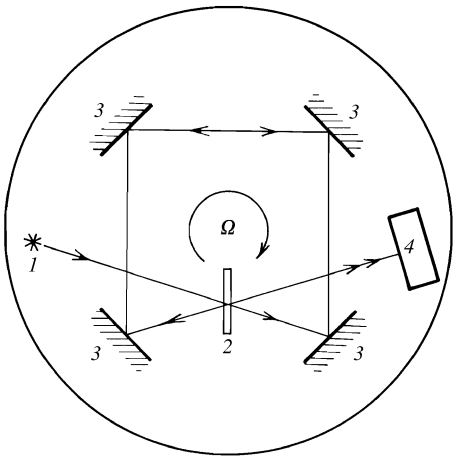

Figure 1. The Sagnac experiment in visible radiation.

Nevertheless by using the postulate of pseudo-Euclidicity of the space–time geometry we can treat the motion of the noninertial system (though without allowing for the dispersion properties of the material media along the path of the rays) within the framework of the special theory of relativity.

In 1925 Michelson and Gale [4, 5] built an apparatus on the principle used in Sagnac's experiment to determine the rate of rotation of the Earth. This required the construction of an interferometer in the form of a rectangle with sides 613 m and 339.5 m.

In 1949 Bershtein [6] produced a variant of Sagnac's experiment using a radio-frequency signal with a frequency of $\omega = 30$ MHz as the information carrier, and a multiturn structure of coaxial cable wound on a drum as the interferometer contour. Because of its essentially novel approach — the replacement of a single circuit of a large system by a multiple circuit of a small system — this work can be considered to be a precursor of the method of realising the Sagnac experiment by using fibre-optical systems (developed in the 1970s) which led to the development of a whole class of phase gyroscopes (fibre-optical detectors) [7].

In 1979 the Sagnac experiment was successfully modified with the aim of determining the rate of rotation of the Earth by means of a purely quantum phenomenon: the phase interference of thermal neutrons circulating (after an initial splitting of the wave function) round a three-mirror interfero-meter of area $S = 9$ cm^2. The Bragg diffraction phenomenon in monocrystalline mirrors was used to produce a closed trajectory for the moving neutrons. Allowing for the form of the de Broglie wave for a moving neutron with $\lambda = 2\pi\hbar/mv$ and for the fact that the trajectories of the two oppositely moving beams in a three-mirror interferometer cover only one half of the total perimeter, one finds that the final expression for the quantum mechanical phase difference becomes

$$\varphi_1 - \varphi_2 = \frac{2mS\Omega}{\hbar} \tag{1.3}$$

and is independent of the velocity and of the energy of the neutron.

The same expression is valid for rotating phase-sensitive interferometers which use the interference of coherent electronic states in superconducting quantum interference devices.

Even when arranged in chronological order the most characteristic models of the Sagnac experiment all have the following features: (a) the use of beams of mutually coherent radiation travelling in opposite directions; (b) systems for forming closed trajectories for these beams; (c) very sensitive phase-sensitive apparatus for detecting rotation.

On purely logical considerations of experiment design these studies of the Sagnac experiment should now be carried out with X-rays or with gamma radiation [9–12].

In addition to offering a more complete methodological approach, i.e. a test for the effect over the whole of the frequency spectrum, these modifications would give (in principle), as a result of the decrease in λ, much more precise characteristics than those obtained in the visible range with an interferometer of the same area. On the other hand the change to electromagnetic radiation of shorter wavelength is technically simpler than using the phenomenon of neutron interference, both for quanta and for monochromatic thermal neutrons of wavelength typical of Bragg diffraction ($\lambda \approx 0.5$–2 A), which can be obtained in reasonable quantities only by monochromatising the flux from nuclear reactors.

Nevertheless, as was shown by calculations and experiments in our laboratories, the formulation of the Sagnac experiment in terms of X radiation meets some very serious difficulties, usually associated with fluctuation effects.

In this review we shall discuss the theoretical aspects of the Sagnac experiment with X radiation and the results of recent experimental studies using a specially constructed apparatus.

Section 2 contains a detailed discussion of the metrological aspects of the noninertial motion of interferometers and resonators, and of the electrodynamics of the wave fields in them, which calls for the use of the elements of general as well as special relativity.

In Section 3 we shall examine the propagation of characteristic waves in the X-ray band and their interaction with a system of monocrystalline mirrors as a function of the determined or fluctuating phase relationships (including those caused by rotation) in the interferometer system.

Sections 4 and 5 are devoted to the formulation, procedure, and results of the experimental realisation of the Sagnac experiment using X radiation.

2. Electrodynamics and metrics of rotating optical systems

Because of the essentially noninertial character of the motion in rotating systems such as that displaying the Sagnac effect a more detailed discussion of the effect should be developed in theoretical terms using the general as well as the special theory of relativity. By adopting this more general approach we shall present the results of studies of the electrodynamics of material media in nonstationary frames of reference specially aimed at detecting the 'vortex optical effect' in the X-ray region.

A clear presentation of the general features of the Sagnac effect, not limited to any particular region of wavelength of the chosen radiation, is obtained by the use of the following model. Let the light from a source be propagated along a circular path in two opposite directions after passing through a splitter (Fig. 2). A suitable ring system can be constructed as a multiple-mirror interferometer, a fibre-optical system, or a closed resonator. If the ring system is at rest relative to the

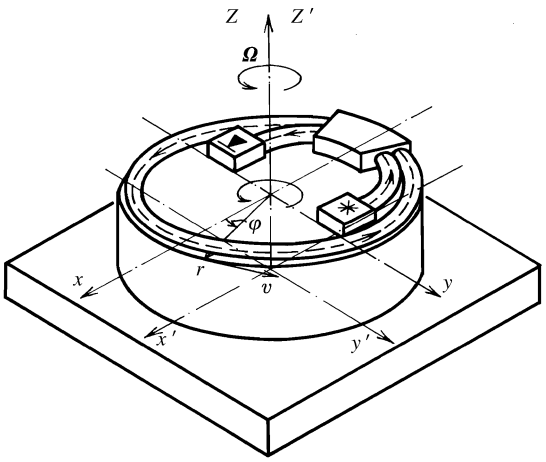

Figure 2. Annular interferometer in a rotating coordinate system.

inertial laboratory frame of reference the two light beams find identical propagation conditions and return to the initial splitter in identical phases. During rotation the propagation conditions of the waves travelling in opposite directions are changed: their velocities are now different, and an additional phase incursion takes place [13].

We shall demonstrate this effect by considering a rotating disc. Let the system K′ be the inertial laboratory system with coordinates $\boldsymbol{r}'$, and the system K be the rotating disc with coordinates $\boldsymbol{r}$. Let us establish the metrics of the rotating disc [14]. The element of length in the radial direction of the disc is identical in the two systems, but the element tangential to the circumference is different. From the point of view of the inertial observer in the system K′ the element along the linear velocity of rotation of the disc should be contracted according to the Lorentz transformation

$$\mathrm{d}l' = \mathrm{d}l(1-\beta^2)^{-1/2}, \quad \boldsymbol{\beta} = \boldsymbol{v}c^{-1}, \quad \boldsymbol{v} = \boldsymbol{\Omega}\times\boldsymbol{r}, \tag{2.1}$$

where $\boldsymbol{v}$ is the linear velocity, $\boldsymbol{\Omega}$ is the angular velocity of the rotation, and c is the velocity of light in a vacuum. The concentric paths of the two systems coincide, but their lengths are different:

$$l = 2\pi r, \quad l' = \oint \mathrm{d}l' = 2\pi r\left[1-\left(\frac{\Omega r}{c}\right)^2\right]^{-1/2} > l\,.$$

Thus, since the familiar expressions of Euclidean geometry are not obeyed on the rotating disc, we must change to a covariant formulation in order to describe adequately the behaviour of an electromagnetic wave. To simplify the calculations we shall consider the propagation of light along the circumference of the rotating disc.

The 4-interval ds for light travelling on the circumference in the inertial system can be written as follows in cylindrical coordinates:

$$\mathrm{d}s^2 = c^2\,\mathrm{d}t'^2 - r'^2\,\mathrm{d}\varphi' = 0\,. \tag{2.2}$$

We shall apply a change of coordinates for the rotating disc:

$$\mathrm{d}t' = \gamma\,\mathrm{d}t, \quad \mathrm{d}\varphi' = \mathrm{d}\varphi + \gamma\Omega\,\mathrm{d}t,$$
$$\gamma = (1-\beta^2)^{-1/2}, \quad r' = r\,. \tag{2.3}$$

Inserting (2.3) into (2.2) gives

$$\mathrm{d}s^2 = [c\,\mathrm{d}t + r(\mathrm{d}\varphi + \gamma\Omega\,\mathrm{d}t)][c\,\mathrm{d}t - r(\mathrm{d}\varphi + \gamma\Omega\,\mathrm{d}t)] = 0\,.$$

As a result we find

$$\mathrm{d}t = r\,\mathrm{d}\varphi\left[\gamma c\left(1 \mp \frac{\Omega r}{c}\right)\right]^{-1}\,. \tag{2.4}$$

Integrating over the whole central angle of the circle gives the change in the time needed by the light beams to circle the perimeter in opposite directions on the rotating disc. The difference between the circulation times of the beams along the perimeter of the rotating disc is defined to first order in angular velocity by the expression

$$\Delta t = t_1 - t_2 = \frac{4\pi r^2\Omega}{c^2} = \frac{4S\Omega}{c^2}\,. \tag{2.5}$$

(We note that this result has also been obtained by other workers [16, 33, 35].) The relative change in the velocity of the wave round the perimeter is $v/c = \Omega r/c$. In the linear approximation, Eqn (2.5) for optical beams can be obtained for any form of flat contour by starting from the vector form of Eqn (2.4):

$$\Delta t = \frac{2}{c^2}\oint_l \boldsymbol{v}\cdot\mathrm{d}\boldsymbol{r} = \frac{2}{c^2}\int\int(\nabla\times\boldsymbol{v})\cdot\boldsymbol{n}\,\mathrm{d}S$$
$$= \frac{4S\boldsymbol{\Omega}\cdot\boldsymbol{n}}{c^2}\,, \tag{2.6}$$

where $\boldsymbol{n}$ is the outward normal to the surface S of the contour, in accordance with the right-hand drill rule $\nabla\times\boldsymbol{v} = 2\boldsymbol{\Omega}$. For two types of ring system (resonator, with full access of both beams travelling in opposite directions to the contour; and the interferometric, with half access) the difference between the times needed for the beams to circle the perimeter produces a change in the phase difference.

The metric of a rotating disc differs from those of inertial systems. In a Cartesian system of coordinates the rotated 3-interval given by

$$\mathrm{d}\boldsymbol{r} = \overline{\overline{R}}\,\mathrm{d}\boldsymbol{r}' + \boldsymbol{v}\,\mathrm{d}t\,,$$
$$\overline{\overline{R}} = \begin{pmatrix} \cos\Omega t, & -\sin\Omega t, & 0 \\ \sin\Omega t, & \cos\Omega t, & 0 \\ 0, & 0, & 1 \end{pmatrix} \tag{2.7}$$

leads to the following expression for the 4-interval:

$$\mathrm{d}s^2 = -c^2\left[1 - \frac{\Omega^2r^2 - (\Omega r)^2}{c^2}\right]\mathrm{d}t^2$$
$$+2|\boldsymbol{\Omega}\times\boldsymbol{r}|\,\mathrm{d}r\,\mathrm{d}t + \mathrm{d}r^2 = g_{\alpha\beta}\,\mathrm{d}x^\alpha\,\mathrm{d}x^\beta\,,$$
$$g_{00} = -(1-\beta^2), \quad g_{0k} = \beta_k, \quad g_{mn} = \delta_{mn}\,. \tag{2.8}$$

The resulting equation (2.8) shows that in order to describe the conditions under which electromagnetic waves are propagated on a rotating platform we must adopt the metrics of noninertial frames of reference. Furthermore the kinematic approach described here is valid only for systems in which the optical channel does not contain additional elements. In the majority of interferometers or resonators the optical channel includes optical elements (plates, phase shifting devices, crystalline structures). Also, since the diffraction is a volume effect in the X-ray region, the substance of the crystal mirrors is unavoidably a component of the optical path. Obviously, however, the initial equations used to describe the state of the electromagnetic waves in rotating systems can only be the Maxwell equations in

covariant form and the corresponding material equations. We introduce the bivectors of the electromagnetic field [15]

$$F^{\mu\nu} = \{F^{0k}\,,\ F^{mn}\} = \{\boldsymbol{D}\,,\boldsymbol{H}\}\,,$$

$$E_{\mu\nu} = \{E_{k0}\,,E_{mn}\} = \{\boldsymbol{E}\,,\boldsymbol{B}\}\,, \tag{2.9}$$

whose components are the 3-dimensional vectors of the electromagnetic displacement and of the field strength. In our notation the Greek indices correspond to the values $\alpha = 0, 1, 2, 3$, and $m = 1, 2, 3$. The Maxwell equations can then be written in terms of the 4-dimensional divergence or the curl of the bivectors of the electromagnetic field:

$$\nabla_\alpha F^{\mu\alpha} = 4\pi j^\mu\,, \qquad \nabla_{[\lambda} E_{\mu\nu]} = 0\,, \tag{2.10}$$

where the 4-dimensional current density vector is related to the electrical charge density and to the 3-dimensional current density by the expression

$$j^\mu = \{j^0\,,\ j^k\} = \left\{\rho\,,\ \frac{\boldsymbol{j}}{c}\right\}. \tag{2.11}$$

In the system of equations (2.10) the covariant derivatives are defined in terms of the connection coefficients, which can themselves be expressed by derivatives of the metric tensor [including the case of rotating systems, Eqn (2.8)]. In the electrodynamics of inertial and of noninertial systems the relationship between the contravariant and covariant bivectors [Eqn (2.9)] is obtained by using the metric tensor, and in electrodynamic media by using the Tamm–Mandelshtam dielectric and magnetic permeability tensor (the D–M tensor). For isotropic media in the characteristic system of a medium inertially at rest this 4-dimensional tensor takes the form

$$\varepsilon^{\mu\nu} = \frac{1}{\mu^{1/2}}\begin{pmatrix} -\varepsilon\mu, & 0, & 0, & 0 \\ 0, & 1, & 0, & 0 \\ 0, & 0, & 1, & 0 \\ 0, & 0, & 0, & 1 \end{pmatrix},$$

$$\varepsilon_{\mu\alpha}\varepsilon^{\alpha\nu} = \delta_\mu^\nu\,; \tag{2.12}$$

Here ε and μ are the dielectric permittivity and the magnetic permittivity respectively. The usual 3-dimensional linking equations $\boldsymbol{D} = \varepsilon\boldsymbol{E}$ and $\boldsymbol{B} = \mu\boldsymbol{H}$ in 4-dimensional form are replaced by the so-called material equations

$$F^{\mu\nu} = \varepsilon^{\mu\alpha}\varepsilon^{\nu\beta}E_{\alpha\beta}\,, \tag{2.13}$$

which are valid in any frame of reference. Only specific information on the fluctuational dependence of the elements of the D–M tensor on the parameters of the medium and of its motion are now required. To determine the form of the components of the D–M tensor it is convenient to apply the conformal dyadic transformations to the metric tensor:

$$\varepsilon^{\mu\nu} = \alpha(g^{\mu\nu} - \kappa u^\mu u^\nu)\,, \qquad \varepsilon_{\mu\nu} = \alpha^{-1}(g_{\mu\nu} + \chi u_\mu u_\nu)\,, \tag{2.14}$$

where u^μ is the 4-velocity of an element of the medium, $\alpha^{-2} = \mu$, $\kappa = \varepsilon\mu - 1$, $\chi = \kappa/(1+\kappa)$. The linking equations (2.13) can be rewritten in terms of the 4th-rank D–M tensors:

$$F^{\mu\nu} = \tfrac{1}{2}\varepsilon^{\mu\nu,\,\alpha\beta}E_{\alpha\beta}\,,$$

$$\tfrac{1}{2}\varepsilon^{\mu\nu,\,\alpha\beta}\varepsilon_{\alpha\beta,\,\gamma\omega} = \delta^{\mu\nu}_{\gamma\omega}\,, \tag{2.15}$$

where

$$\varepsilon^{\mu\nu,\,\lambda\sigma} = 2\varepsilon^{[\mu|\lambda}\varepsilon^{\nu]\sigma} = 2\alpha^2\left(g^{[\mu|\lambda}g^{\nu]\sigma} + 2\kappa u^{[\lambda}g^{\sigma][\mu}u^{\nu]}\right).$$

The 4th-rank D–M tensors (2.15) are very cumbersome. However, if we allow for their symmetry only 36 of their 256 elements remain linearly independent. To simplify the discussion it is convenient to describe the material equations (2.15) in the 6-dimensional space of the electromagnetic field bivectors. We shall introduce the collective indices of the 6-dimensional (configurations) space [14], $A = \{01; 02; 03; 23, 31, 12\}$. After this the bivectors of the electromagnetic field (2.9) can be represented in the 6-dimensional space by means of a single-row column or a six-row line:

$$E^A = \{E^{0k}\,,E^{mn}\} = \{\boldsymbol{D},\boldsymbol{H}\}\,,$$

$$E_A = \{E_{0k}\,,E_{mn}\} = \{-\boldsymbol{E},\boldsymbol{B}\}\,. \tag{2.16}$$

As a result the 4th-rank D–M tensors in the 4-dimensional space become 2nd-rank in the 6-dimensional bivectors space. This simplifies the formulation of the material equations. In the corresponding system composed of even an anisotropic medium the 6-dimensional D–M tensors take a simple form, convenient for comparisons with the usual 3-dimensional tensors of the dielectric constant ($\overline{\overline{\varepsilon}}$) and the magnetic permeability ($\overline{\overline{\mu}}$)

$$\varepsilon^{A,B} = \left(\begin{array}{c|c} -\overline{\overline{\varepsilon}} & 0 \\ \hline 0 & \overline{\overline{\mu}}^{-1} \end{array}\right);$$

$$\varepsilon_{A,B} = \left(\begin{array}{c|c} -\overline{\overline{\varepsilon}}^{-1} & 0 \\ \hline 0 & \overline{\overline{\mu}} \end{array}\right). \tag{2.17}$$

Here the 6-dimensional matrices are broken down into four 3-dimensional blocks. The constraint equations (2.13) on the bivectors of the electromagnetic field finally take the form

$$E^A = \varepsilon^{A,B}E_B\,, \qquad \varepsilon^{A,B}\varepsilon_{B,C} = \delta^A_C\,. \tag{2.18}$$

The conformational dyadic transformations (2.14) for the metric tensor in 6-dimensional form do not undergo marked changes and now become

$$\varepsilon^{A,B} = \alpha^2(g^{A,B} - \kappa u^{A,B})\,, \qquad u^{A,B} = 2u^{[\lambda}g^{\sigma][\mu}u^{\nu]}\,, \tag{2.19}$$

By using the definitions (2.19) and (2.17) we can calculate the 6-dimensional D–M tensor in the corresponding rotating disc system:

$$\varepsilon^{A,B} = \left(\begin{array}{c|c} -(\overline{\overline{\varepsilon}}\,\overline{\overline{g}}^{-1} - \overline{\overline{\mu}}^{-1}\overline{\overline{\beta}}) & -\overline{\overline{\mu}}^{-1}\overline{\overline{V}} \\ \hline \overline{\overline{\mu}}^{-1}\overline{\overline{V}} & \overline{\overline{\mu}}^{-1}\,\overline{\overline{g}} \end{array}\right),$$

$$\overline{\overline{V}} = \begin{pmatrix} 0, & 0, & \beta_y \\ 0, & 0, & -\beta_z \\ -\beta_y, & \beta_x, & 0 \end{pmatrix},$$

$$\varepsilon_{A,B} = \left(\begin{array}{c|c} -\overline{\overline{\varepsilon}}^{-1}\,\overline{\overline{g}} & -\overline{\overline{\varepsilon}}^{-1}\overline{\overline{V}} \\ \hline \overline{\overline{\varepsilon}}^{-1}\overline{\overline{V}} & \overline{\overline{\mu}}\,\overline{\overline{g}}^{-1} - \overline{\overline{\varepsilon}}^{-1}\beta \end{array}\right),$$

$$\overline{\overline{g}} = \begin{pmatrix} 1-\beta_y^2, & \beta\beta_y, & 0 \\ \beta_x\beta_y, & 1-\beta_x^2, & 0 \\ 0, & 0, & 1-\beta^2 \end{pmatrix},$$

$$\overline{\overline{\beta}} = \frac{1}{1-\beta^2}\begin{pmatrix} \beta_y^2, & -\beta_x\beta_y, & 0 \\ -\beta_x\beta_y, & \beta_x^2, & 0 \\ 0, & 0, & \beta^2 \end{pmatrix}. \tag{2.20}$$

The block structure of the 6-dimensional matrices allows us to pass relatively easily from the bivector form of the material equations (2.18) to the 3-dimensional (vector) form. In the special case of isotropic media these equations for the electric displacement and the field intensity simplify to

$$\boldsymbol{D} = \varepsilon \bar{\bar{g}}^{-1}\boldsymbol{E} - \gamma^2 \boldsymbol{\beta} \times \boldsymbol{H}, \quad \boldsymbol{B} = \mu \bar{\bar{g}}^{-1}\boldsymbol{H} + \gamma^2 \boldsymbol{\beta} \times \boldsymbol{E} . \quad (2.21)$$

Analogous expressions can be obtained not only for material media but also for material systems in the field of rotating masses. For example, for the Kerr metric [16] and for the case of a field far from the centre of mass, when $r \gg r_g \equiv 2\gamma m/c^2$, the 4-interval in the local Cartesian system of coordinates becomes

$$\begin{aligned} \mathrm{d}s^2 &= -c^2(1 - r_g r^{-1})\,\mathrm{d}t^2 + \mathrm{d}x^2(1 - r_g r^{-1})^{-1} \\ &\quad + \mathrm{d}y^2 + \mathrm{d}z^2 + 2r_g r^{-2} a_r c t\,\mathrm{d}z , \end{aligned} \quad (2.22)$$

where the constant $a_r = a \sin\theta$ is proportional to the angular momentum component. By using the metric tensor of (2.22) we can obtain its 6-dimensional construction. Material equations of the type of (2.18) produce the following 3-dimensional equations similar to (2.21):

$$\begin{aligned} &\boldsymbol{D} = \bar{\bar{N}}(\boldsymbol{E} - \bar{\bar{\bar{W}}}\boldsymbol{H}), \quad \boldsymbol{B} = \bar{\bar{N}}(\boldsymbol{H} + \bar{\bar{\bar{W}}}\boldsymbol{E}) , \\ &\bar{\bar{N}} = \begin{pmatrix} 1, & 0, & 0 \\ 0, & (1 - r_g r^{-1})^{-1}, & 0 \\ 0, & 0, & (1 - r_g r^{-1})^{-1} \end{pmatrix} , \\ &\bar{\bar{\bar{W}}} = W \begin{pmatrix} 0, & -1, & 0 \\ 1, & 0, & 0 \\ 0, & 0, & 0 \end{pmatrix}, \quad W = r_g a_r r^{-2} . \end{aligned} \quad (2.23)$$

In the case of a nonrotating gravitational mass the corresponding angular momentum $|\boldsymbol{M}| = mca \to 0$, and the Kerr metric is replaced by the Schwartzchild metric while the 3-dimensional tensors $\bar{\bar{\bar{W}}} \to 0$. As a result the constraint equations (2.23) reduce to the usual material equations only for electrical or only for magnetic field vectors. Thus, the effect of rotation in the first order of angular velocity can be obtained in the final formulae by using the constraint equation for the electric displacement and field intensity with the additional terms (2.21) or (2.23).

In the general case the system of Maxwell equations (2.10) with the material equations (2.21) is unwieldy because of the dependence of the permittivity tensors in the rotating system on the coordinates. In many cases the system can be simplified. Thus, in the geometrical optics approximation we can ignore the changes in the field parameters and in those of the medium in the transverse plane of the wave fronts of the electromagnetic waves. Then in the local region of waves propagated along the linear rotation velocity the solutions for plane waves remain valid:

$$\begin{aligned} &\boldsymbol{E} = \boldsymbol{E}_0 \exp[\mathrm{i}(\omega t - \boldsymbol{k} \cdot \boldsymbol{r})] , \\ &|\boldsymbol{E}_0| = \mathrm{const}, \quad \boldsymbol{k} = \frac{\boldsymbol{\xi}\omega}{c} , \end{aligned} \quad (2.24)$$

where $\boldsymbol{k}$ is the wave vector and $\boldsymbol{\xi}$ are the vectors of normal refraction, equal in modulus to the refractive index.

The differential equations for the free electro-magnetic field take the vectorial form

$$\begin{aligned} &\boldsymbol{D} = -\boldsymbol{\xi} \times \boldsymbol{H}, \quad \boldsymbol{B} = \boldsymbol{\xi} \times \boldsymbol{E}, \\ &\boldsymbol{\xi} \cdot \boldsymbol{D} = 0, \quad \boldsymbol{\xi} \cdot \boldsymbol{B} = 0 , \end{aligned} \quad (2.25)$$

with the material equations (2.21). Simultaneous solution of (2.25) and (2.21) gives the effective dielectric and magnetic permittivity tensors

$$\begin{aligned} &\boldsymbol{D} = \bar{\bar{\varepsilon}}_{\mathrm{eff}}\boldsymbol{E}, \quad \boldsymbol{B} = \bar{\bar{\mu}}_{\mathrm{eff}}\boldsymbol{H} , \\ &\bar{\bar{\varepsilon}}_{\mathrm{eff}} = \left(\bar{\bar{n}} - \overleftrightarrow{\beta}\overleftrightarrow{\xi}\right)\mu^{-1}, \quad \bar{\bar{\mu}}_{\mathrm{eff}} = \left(\bar{\bar{n}} - \overleftrightarrow{\beta}\overleftrightarrow{\xi}\right)\varepsilon^{-1} , \end{aligned} \quad (2.26)$$

where the following 3-dimensional tensors have been used:

$$\begin{aligned} &\boldsymbol{a} \times \boldsymbol{b} \equiv \overleftrightarrow{a}\boldsymbol{b} \\ &\bar{\bar{n}} = \gamma^2 \begin{pmatrix} (\varepsilon\mu - \beta^2) - \beta_1^2(\varepsilon\mu - 1), & -(\varepsilon\mu - 1)\beta_1\beta_2, & 0 \\ -(\varepsilon\mu - 1)\beta_1\beta_2, & (\varepsilon\mu - \beta^2) - \beta_2^2(\varepsilon\mu - 1), & 0 \\ 0, & 0, & \varepsilon\mu - \beta^2 \end{pmatrix}, \\ &\overleftrightarrow{a} = \begin{pmatrix} 0, & -a_3, & a_2 \\ a_3, & 0, & -a_1 \\ -a_2, & a_1, & 0 \end{pmatrix} . \end{aligned} \quad (2.26a)$$

The ordinary refraction vector is found by solving the equation when the determinant of the uniform system of equations for the strength of the electromagnetic field vanishes:

$$\left| \left(\overleftrightarrow{\xi}\bar{\bar{g}}\overleftrightarrow{\xi} + \varepsilon\mu\bar{\bar{g}}^{-1} + \gamma^2\overleftrightarrow{\beta}\overleftrightarrow{\beta} \right) - \left(\overleftrightarrow{\xi}\overleftrightarrow{\beta} + \overleftrightarrow{\beta}\overleftrightarrow{\xi} \right) \right| = 0 . \quad (2.27)$$

In the special case of the propagation of a wave along the ring system, when the wave vector is parallel to the linear velocity of rotation in every local region, we obtain a solution for a plane wave with a wave resistance $R = |\boldsymbol{E}|/|\boldsymbol{H}| = (\mu/\varepsilon)^{1/2}$, for which the ordinary refraction vector is transformed according to the law

$$\xi = (\xi_0 + \beta)(1 - \beta^2)^{-1}, \quad \xi_0 = (\varepsilon\mu)^{1/2} . \quad (2.28)$$

The result (2.28) is the basis for the determination of the phase difference between waves travelling round the perimeter in opposite directions in the Sagnac experiment in the case of a resonator and an interferometer respectively:

$$\begin{aligned} \varphi_0 &= \pm 4\pi S\Omega\left[\lambda c(1 - \beta^2)\right]^{-1} , \\ \varphi_0 &= \pm 2\pi S\Omega\left[\lambda c(1 - \beta^2)\right]^{-1} . \end{aligned} \quad (2.29)$$

This same change in the effective refractive index $|\boldsymbol{\xi}|$ for two waves circulating in opposite directions leads (as a result of the difference in the optical lengths of the resonator perimeter) to a difference in the characteristic resonance frequencies:

$$\omega = \omega_0\left(1 \pm \frac{\Omega r}{c}\right)(1 - \beta^2) . \quad (2.30)$$

In an actual annular interferometer or resonator a transverse mode structure which makes the wave inhomogeneous and different from the solution (2.24) can be formed. This phenomenon can be allowed for by solving the system of Maxwell equations (2.10) simultaneously with the material equations in the quasioptical approximation [17].

In a rotating system with a 3-dimensional formulation in Cartesian coordinates the Maxwell equations stay the same as in an immobile system if all four vectors of the electromagnetic field remain in their places. Allowing for the material expressions (2.21) the system of Maxwell equations reduces to equations for the electric and magnetic field intensity vectors:

$$\left(\nabla+\boldsymbol{\beta}\frac{1}{c}\frac{\partial}{\partial t}\right)\times\boldsymbol{H}=\frac{4\pi}{c}\boldsymbol{j}+\frac{\varepsilon}{c}\frac{\partial}{\partial t}\boldsymbol{E}\,,$$

$$\left(\nabla+\boldsymbol{\beta}\frac{1}{c}\frac{\partial}{\partial t}\right)\times\boldsymbol{E}=-\frac{\mu}{c}\frac{\partial}{\partial t}\boldsymbol{H}\,,$$

$$\left(\nabla+\boldsymbol{\beta}\frac{1}{c}\frac{\partial}{\partial t}\right)\cdot\boldsymbol{E}=\frac{4\pi}{c}\left(\rho-\frac{\boldsymbol{\beta}\cdot\boldsymbol{j}}{c}\right)\,,$$

$$\left(\nabla+\boldsymbol{\beta}\frac{1}{c}\frac{\partial}{\partial t}\right)\cdot\boldsymbol{H}=0\,. \tag{2.31}$$

For a toroidal regular resonator the solution with a slowly varying field amplitude is

$$\boldsymbol{E}_p(\boldsymbol{r})=\boldsymbol{e}_p(\boldsymbol{r})\exp(-\mathrm{i}hq)\,, \tag{2.32}$$

in which q is the longitudinal coordinate along the perimeter of the toroid and h is the longitudinal wave number. This solution leads to the following equation for the spectrum of characteristic frequencies:

$$K_\perp^2=h_p^2-(h_p-\omega_p\beta c^{-1})^2\,. \tag{2.33}$$

Here $K_\perp$ is the transverse wave number, determined by the transverse mode structure of the field and the transverse dimensions of the waveguide part of the resonator.

In the geometrical optics approximation, in which the transverse structure can be ignored, we have $K_\perp\to 0$, and for the longitudinal wave number we obtain the expression

$$h_p=\omega_p[(\varepsilon\mu)^{1/2}+\beta]c^{-1}\,, \tag{2.34}$$

the analogue of (2.28) for plane waves with a uniform structure in the first order of the linear velocity of rotation.

For a quasioptical annular resonator of radius r_0, in which the oscillatory field is limited by caustics of size d, the dispersion relationship for the characteristic waves and frequencies takes the form

$$2K_\perp d=m\pi+(2n+1)\arcsin(\tanh\eta)\,, \tag{2.35}$$

where

$$K_\perp^2=h_p-\left(\frac{m}{r_0}-\frac{\beta\omega_0}{c}\right)^2\,,$$

$$h_p=\frac{\omega_p(\varepsilon\mu)^{1/2}}{c}\,,\qquad \tanh\eta=\left(\frac{d}{r_0}\right)^{1/2}\,, \tag{2.35a}$$

and the integers ρ, m, and n define the number of wave or half-wave oscillations of the field (respectively) along the perimeter and in the transverse direction.

Thus, the existing equations of the electrodynamics of media in rotating frames of reference can be used to calculate the phase changes in interferometers or the frequency beats in annular resonators with an active medium produced by the rotation of the platform, and also parameters such as the dielectric constant and magnetic permeability in the optical channels or in the design of the system. In particular the effect of rotation is seen not only in the phase (2.29) and the frequency characteristics (2.30) but also in the effective susceptibility of the medium, obtained from (2.28) and given by

$$\chi_{\mathrm{eff}}\equiv\varepsilon_{\mathrm{eff}}-1\equiv|\xi|-1\cong\chi+2\beta\,. \tag{2.36}$$

In the X-ray region χ_{eff} effectively determines all the characteristics of the Bragg diffraction (the fundamental effect in the X-ray analogue of the Sagnac experiment). It can be seen that in the X-ray region, which is characterised by a very low value of $|\chi|\ll 1$, the effect of the relativistic factor is observed at lower values of $\beta\ll 1$ and becomes predominant for $\beta>|\chi|/2$, whereas in the optics of the visible region a comparable effect is obtained only in motions whose velocity approaches the speed of light. In the problems with $|\beta|\ll|\chi|$, discussed below, we shall assume that $\chi_{\mathrm{eff}}\approx\chi$.

3. Electrodynamics of the characteristic waves in a crystalline X-ray resonator or interferometer allowing for rotation

All the conditions stipulated for the realisation of the Sagnac experiment in the X-ray region (formation of coherent waves, formation of a closed ring trajectory, effective phase-sensitive detectors) can be satisfied automatically in a multimirror crystalline interferometer or resonator.

Let us examine the special features of the electrodynamics of characteristic waves in crystalline periodic structures.

The solution of the wave equation

$$\nabla^2\boldsymbol{E}(\boldsymbol{r},t)-\frac{1}{c^2}\frac{\partial^2}{\partial t^2}\boldsymbol{E}(\boldsymbol{r},t)=\frac{4\pi}{c^2}\frac{\partial^2}{\partial t^2}\left[\overleftrightarrow{\chi}(\boldsymbol{r})\boldsymbol{E}(\boldsymbol{r},t)\right] \tag{3.1}$$

in crystals is a set of characteristic waves corresponding to the expansion of $\boldsymbol{E}(\boldsymbol{r},t)$ into a Fourier series of the reciprocal lattice vectors $\boldsymbol{K}_n=n\boldsymbol{K}$:

$$\boldsymbol{E}(\boldsymbol{r},t)=\sum_{n,i}\boldsymbol{e}_n^i E_n^i\exp\left[\mathrm{i}(\omega t-\boldsymbol{k}_n\cdot\boldsymbol{r})\right]\,, \tag{3.2}$$

where $\boldsymbol{k}_n=\boldsymbol{k}_0+\boldsymbol{K}_n$, $\omega=2\pi c/\lambda$, and $\boldsymbol{e}_n$ is the unit vector of the polarisation of the electromagnetic wave travelling in the direction of the vector $\boldsymbol{k}_n$.

By ignoring the small longitudinal components of $\boldsymbol{E}(\boldsymbol{r},t)$ in the crystal [18] and using the expansion (3.1) we can easily convert Eqn (2.1) into

$$\sum_n(k_n^2-\omega^2c^{-2})E_n^i\exp\left[\mathrm{i}(\omega t-\boldsymbol{k}_n\cdot\boldsymbol{r})\right]$$

$$=\frac{4\pi\omega^2}{c^2}\sum_{\beta,l}\chi^{il}(r)E_\beta^l\exp\left[\mathrm{i}(\omega t-\boldsymbol{k}_\beta\cdot\boldsymbol{r})\right]\,, \tag{3.3}$$

where $\chi^{il}(\boldsymbol{r})$ is the tensor of the local susceptibility of the crystal. Multiplying this equation by $\exp[-\mathrm{i}(\omega t-\boldsymbol{k}_\alpha\cdot\boldsymbol{r})]$ and integrating over the volume of the unit cell V_0 of the crystal we obtain

$$(\boldsymbol{k}_\alpha^2\kappa^{-2}-1)E_\alpha^i=\sum_{\beta,l}g_{\alpha\beta}^{il}E_\beta^l\,,$$

$$g_{\alpha\beta}^{il}=\frac{4\pi}{V_0}\int_{V_0}\chi^{il}(r)\exp\left[\mathrm{i}(\boldsymbol{k}_\alpha-\boldsymbol{k}_\beta)\cdot\boldsymbol{r}\right]\mathrm{d}V\,, \tag{3.4}$$

where $g_{\alpha\beta}^{il}$ is a tensor with components proportional to the Fourier density of the local susceptibility of one unit cell, and $\kappa=\omega/c$. The quantity $g_{\alpha\beta}^{il}$ corresponds essentially to the amplitude scattering of the wave E_α^i into the wave E_β^l for one unit cell.

Allowing for the specific parameters of the γ transition in the nucleus and of the electronic transition in the atom the explicit expression for $g_{\alpha\beta}^{il}$ can be converted into the general form [19]

$$g^{il}_{\alpha\beta} = \tilde{\chi}^{il}_{\alpha\beta} + \chi^{il}_{\alpha\beta} ,$$
$$\chi^{il}_{\alpha\beta} = r_0 F_{\alpha\beta}(|\boldsymbol{k}_\alpha - \boldsymbol{k}_\beta|) p^{il}(\theta_\alpha, \varphi_\alpha; \theta_\beta, \varphi_\beta) ,$$
$$\tilde{\chi}^{il}_{\alpha\beta} = \tilde{\chi}_{0\alpha\beta} \sum_{M, M_0} C^{JM}_{j_0 LM\,(M-M_0)} C^{J_0 M_0}_{JLM\,(M_0-M)} \times \frac{[\boldsymbol{X}^{M-M_0}_L(\theta_\alpha, \varphi_\alpha)\boldsymbol{e}^i_\alpha][\boldsymbol{X}^{M_0-M}_L(\theta_\beta, \varphi_\beta)\boldsymbol{e}^l_\beta]}{\mathrm{i} + [2(\omega - \omega_{M,M_0})/\Gamma]} . \quad (3.5)$$

Here r_0 is the classical radius of the electron; $F_{\alpha\beta}$ is the atomic factor; p^{il} is the polarisation factor for electron scattering; $C^{J_2 M_2}_{J_1 L M_1 (M_2 - M_1)}$ are the Klebsch–Jordan coefficients; $\boldsymbol{X}^{M_2-M_1}_L(\theta_\alpha, \varphi_\alpha)$ is the vectorial spherical harmonic for the electromagnetic transition of the multiplicity L between the hyperfine sublevels of the nucleus with spin projections on the quantisation axis M_1 and M_2; $\boldsymbol{e}^i_\alpha$ are the polarisation vectors of the characteristic waves E^i_α lying in the scattering plane ($i = 2$) or in a plane at right angles to it ($i = 1$); θ_α and φ_α are spatial angles describing the orientation of the vector $\boldsymbol{k}_\alpha$; $\tilde{\chi}_{0\alpha\beta}$ is a parameter which allows for the relative concentration of resonance nuclei, the Mössbauer factor, and the position of the resonance nucleus in the unit cell [20].

For resonance processes involving the Mössbauer gamma radiation we have $|\tilde{\chi}^{il}_{\alpha\beta}| \gg |\chi^{il}_{\alpha\beta}|$.

In the cases of greatest practical importance the system of linear equations (3.4) is greatly simplified.

If the direction $\boldsymbol{k}_0$ of the wave E^i_0 falling on the crystal does not satisfy the Bragg condition,which in this case corresponds to the requirements that $\boldsymbol{k}_\alpha - \boldsymbol{k}_0 = \pm \boldsymbol{K}_n$, the integral over the volume of the unit cell in the expressions for $g^{il}_{\alpha\beta}$ is different from zero only in the case of scattering without change in the direction of the wave. As a result the problem reduces to the rectilinear propagation of a wave in an anisotropic medium.

The next simplest case, which is very important in practice, is when the Bragg condition is obeyed for only one of the scattered waves with wave vector $\boldsymbol{k}_1 = \boldsymbol{k}_0 \pm \boldsymbol{K}$. Under these conditions only the amplitudes of the characteristic waves E^i_0 and E^l_1 are different from zero. These waves are related by the system of four equations

$$(k^2_\alpha \kappa^{-2} - 1) E^i_\alpha = \sum_{l=1}^{2} \sum_{\beta=0}^{1} g^{il}_{\alpha\beta} E^l_\beta ,$$
$$i = 1, 2, \quad \alpha = 0, 1 . \quad (3.6)$$

Putting, as usual [18], $k_0 = \kappa(1 + \varepsilon)$, $k_1 = \kappa(1 + b\varepsilon + \delta/2)$, where $|\varepsilon| \ll 1$, $b = \cos\theta_0 / \cos\theta_1$, and $\delta = \boldsymbol{K} \cdot (\boldsymbol{K} + 2\boldsymbol{\kappa})/\kappa^2$ is a small angular deviation of the direction of incidence of the wave on the crystal from the exact Bragg condition, we obtain from the condition that the determinant of the system (3.6) must be zero a fourth-order dispersion equation which defines the complex quantity ε (which characterises, in particular, the absorption of the waves). In general this solution cannot be obtained in an explicit form. Some special cases in which ε can be found have been discussed [18–20]. The equation for ε can be simplified substantially in the simplest case of external fields acting on the scattering nucleus or atom, or in the presence of an internal perturba-tion having an energy whose eigenvalues are independent of the sign of the projection of the spin of the scattering nucleus on the quantisation axis. For example, the latter condition is satisfied by the quadrupole interaction of the momentum of the nucleus with the electrostatic field of the lattice. Under these conditions the expression for $g^{il}_{\alpha\beta}$ [Eqn (3.5)] is diagonalised with respect to the polarisation indices, and $g^{il}_{\alpha\beta} = g^{il}_{\alpha\beta}\delta_{il}$. As a result the system (3.6) is split into two independent subsystems containing two equations each for different polarisations of the field:

$$(k^2_\alpha \kappa^{-2} - 1) E^i_\alpha = \sum_{\beta=0}^{1} g^{ii}_{\alpha\beta} E^i_\beta , \quad \alpha = 0, 1 , \quad (3.7)$$

and the solution of the dispersion equation for this system is

$$\varepsilon^i_{1,2} = \tfrac{1}{4}(g^{ii}_{00} + b g^{ii}_{11} - b\delta) \mp \tfrac{1}{4}\left[(g^{ii}_{00} + b g^{ii}_{11} - b\delta)^2 + 4b(g^{ii}_{00}\delta - \Delta^i)\right]^{1/2} ,$$
$$\Delta^i = g^{ii}_{00} g^{ii}_{11} - g^{ii}_{01} g^{ii}_{10} . \quad (3.8)$$

The appearance of two wave vectors $\boldsymbol{k}(\varepsilon^i_1), \boldsymbol{k}(\varepsilon^i_2)$ for the refracted as well as for the reflected wave is associated with the relief of the degeneracy in wave number space, owing to an interaction of the waves in the crystal. The explicit form of $\varepsilon^i_{1,2}$ depends on the characteristic parameter Δ^i. It follows from (3.5) that in the case of an E1 electrical dipole transition $g^{11}_{00} = g^{11}_{11} = g^{11}_{01} = g^{11}_{10}$ in the scattering nucleus, and Δ^i for a wave polarised at right angles to the scattering plane, whereas, as in the case of the wave polarised in the scattering plane, we have

$$g^{22}_{00} = g^{22}_{11} = g^{22}_{01}(\cos 2\theta_0)^{-1} = g^{22}_{10}(\cos 2\theta_0)^{-1} ,$$
$$\Delta^2 = (g^{22}_{00})^2 \sin^2 2\theta_0 . \quad (3.8a)$$

For a magnetic dipole transition of the M1 type involving Mössbauer radiation with $|\tilde{\chi}^{il}_{\alpha\beta}| \gg |\chi^{il}_{\alpha\beta}|$ we have $\Delta^2 = 0$, $\Delta^1 = (g^{11}_{00}) \sin^2 2\theta_0$.

In both these types of transition with a wave E^i_0 incident on the crystal in the exact Bragg direction for which $\delta = 0$ and with a polarisation corresponding to the condition $\Delta^i = 0$ we have

$$\varepsilon^i_1 = 0 , \quad \varepsilon^i_2 = \tfrac{1}{2} g^{ii}_{00}(1 + b) . \quad (3.8b)$$

The vanishing of one of the roots, ε^i_1, (which defines the imaginary part of $\boldsymbol{k}_\alpha$) shows that a wave with this polarisation creates, as a result of diffraction in the bulk of the crystal, a coherent superposition of a refracted (wave vector $\boldsymbol{k}_0$) and a diffracted wave [wave vector $\boldsymbol{k}_1$, Eqn (3.3)], which passes through the crystal (case of diffraction in the Laue geometry) or is reflected from it (diffraction in the Bragg geometry) without loss in either case. At the same time the second root $\varepsilon^i_1 > g^{ii}_{00}$ for the Laue diffraction ($b > 0$) corresponds to a superposition of the waves which is strongly absorbed in the crystal.

Comparing the latter root, ε^i_2, with the solution (3.8), obtained for angles differing substantially from the Bragg angle but equal ($\varepsilon^i = g^{ii}_{00}/2$), we can see that this form of the solution predicts a spatial attenuation of the superposition with a decrement $(1 + b)$ times greater than for a wave propagated outside the limits of the Laue diffraction region.

However, in the case of Bragg diffraction the second root of the dispersion equation is $\varepsilon^i_2 \ll g^{ii}_{00}/2$, and in the case of symmetrical diffraction with $b = -1$ it vanishes. This result suggests the possibility of the almost complete exclusion of bulk absorption for the whole of the incident radiation with a given polarisation for symmetrical reflection from the surface, and the realisation of this effect for only part (approximately one half) of the incident radiation, corresponding to the ε^i_1 (first) root for the Laue diffraction, when the incident wave and the sum of the refracted and the

diffracted waves lie on different sides of the crystal. Obviously, the Bragg diffraction can be used to create a very efficient reflecting mirror with a reflection coefficient $R \approx 1$, whereas the Laue diffraction can be used in a coherent splitter of short-wave radiation, and also (in many cases) to produce a reflecting mirror.

Let us examine in an explicit form the structure of the field in the Laue geometry. In this case we obtain from (3.7)

$$E_1^i(\varepsilon_{1,2}^i) = \left[(2\varepsilon_{1,2}^i - g_{00}^{ii})(g_{01}^{ii})^{-1}\right] E_0^i(\varepsilon_{1,2}^i) \ . \qquad (3.8c)$$

From this expression we find, for waves being propagated in the exact Bragg direction with $\Delta^i = 0$, one obtains

$$E_1^i(\varepsilon_1^i) = -E_0^i(\varepsilon_1^i) \ , \quad E_1^i(\varepsilon_2^i) = E_0^i(\varepsilon_2^i) \ ,$$

$$E_0^i(\varepsilon_1^i) = E_0^i(\varepsilon_2^i) = \frac{\tilde{E}_0}{2} \ , \qquad (3.9)$$

where $\tilde{E}_0$ is the amplitude of the wave incident on the crystal.

Allowing for (3.9) gives the following solution of (3.3):

$$E^i(r, t) = \left[E_0^i(\varepsilon_1^i) + E_1^i(\varepsilon_1^i) \exp(\mathrm{i}\boldsymbol{K}\cdot\boldsymbol{r})\right] \times \exp\left[\mathrm{i}(\omega t - \boldsymbol{k}_0(\varepsilon_1^i)\cdot\boldsymbol{r})\right] + \left[E_0^i(\varepsilon_2^i) + E_1^i(\varepsilon_2^i)\right] \times \exp(\mathrm{i}\boldsymbol{K}\cdot\boldsymbol{r}) \exp\left[\mathrm{i}(\omega t - \boldsymbol{k}_0(\varepsilon_2^i)\cdot\boldsymbol{r})\right] \ , \qquad (3.10)$$

resulting from the presence of two types of superposition of the characteristic waves.

The first superposition of the refracted and the diffracted wave, which corresponds to the root ε_1^i, vanishes in the regions of the crystal associated with the crystal planes, for which $\boldsymbol{K}\cdot\boldsymbol{r} = 2\pi$. Since the great majority of the atomic electrons and all the nuclei are located close to these planes this produces a very marked suppression of the absorption process, analytically displayed by the form of the decay to zero of the imaginary part of the wave vectors $\boldsymbol{k}_0(\varepsilon_1^i)$ and $\boldsymbol{k}_1(\varepsilon_1^i)$.

For the second superposition with $\boldsymbol{K}\cdot\boldsymbol{r} = 2\pi$ the amplitude of the combined fields (for symmetrical diffraction) is equal to double the amplitude of each of the waves, which doubles the absorption coefficient for this pair of waves, leading to its complete decay in a layer $1-10$ μm thick (for Mössbauer radiation) or hundreds of micrometres thick (for an X-ray wave).

The final conclusion, as in the qualitative considerations examined above, is that the initial incident wave is split in the crystal into two very slowly decaying coherent waves having half their previous amplitude and diverging at double the Bragg angle ($2\theta_0$).

At low deviations ($\delta \neq 0$) of the direction of the incident wave from the exact Bragg angle the condition (3.9) no longer applies, and the amplitudes of both diffracted waves $E_1^i(\varepsilon_{1,2}^i)$ and refracted waves $E_0^i(\varepsilon_{1,2}^i)$ increases, ultimately leading to incomplete compensation of the first superposition within the plane and to an increased absorption. In the limit of a very large angular deviation the amplitudes of the diffracted waves become negligibly small and the problem reduces to the single-wave case. This effect (suppression of the absorption near the Bragg direction) was first detected by Borman [21] in the case of X-rays, and predicted by Kagan and Afans'ev [18] for Mössbauer radiation.

By using these features of the electrodynamics of short-wave radiation in monocrystals we can analyse proposed [9–11] schemes for setting up the Sagnac experiments, one of which has been realised in practice.

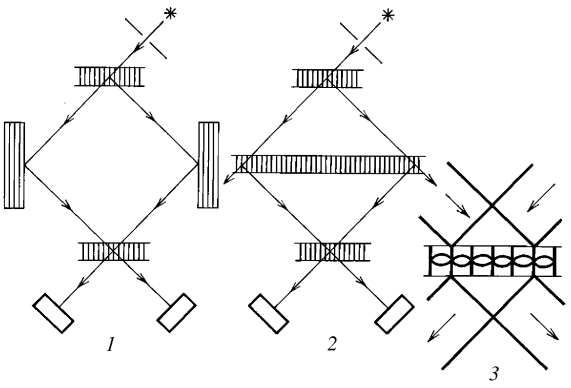

Figure 3. Path of the rays in a three-mirror crystal interferometer with reflecting mirrors in the Bragg (*1*) and the Laue geometry (*2*); (*3*) shows the structure of the interference field in the volume of the emergence mirror.

The initial radiation from the source through a system of collimating diaphragms falls on a monocrystalline plate fixed in the Bragg position with respect to the direction of the source. The formation of a weakly absorbing wave superposition leads to the creation within the crystal of two coherent waves of equal amplitude emerging from the crystal in the $\boldsymbol{\kappa}$ and $\boldsymbol{\kappa}_1 = \boldsymbol{\kappa} + \boldsymbol{K}$ directions:

$$E^i(\boldsymbol{r}, t) = E_0^i(\varepsilon_1^i) \exp\left[\mathrm{i}(\omega t - \boldsymbol{\kappa}\cdot\boldsymbol{r})\right] + E_1^i(\varepsilon_1^i) \exp\left[\mathrm{i}(\omega t - \boldsymbol{\kappa}_1\cdot\boldsymbol{r})\right] \ ,$$

$$\boldsymbol{\kappa} = \boldsymbol{k}_0(\varepsilon_{1,2} = 0) \ . \qquad (3.10a)$$

Crystalline reflecting mirrors in the Bragg [Fig. (3a)] or in the Laue geometry [Fig. (3b)] are used to ensure the spatial convergence of these waves. In the latter case each of the incident waves (in turn) is split on this mirror into a coherent pair identical to the initial pair. Only one wave from each of these pairs is used in the subsequent interference in the third crystal. The two unreflected waves can be used in a control (monitoring) channel after passing through the reflecting mirror.

We note that for very thin crystals of thickness $L = L_p$, in which

$$L_p = (2p+1)\pi \cos\theta_0 \left|\mathrm{Re}\left[k_0^i(\varepsilon_1^i) - k_0^i(\varepsilon_2^i)\right]\right|^{-1} \ ,$$

$$L_p < \cos\theta_0 \left|\mathrm{Im}\, k_0^i(\varepsilon_{1,2}^i)\right|^{-1} , \quad p = 0, 1, 2, \ldots \ , \qquad (3.10b)$$

the incident wave is completely transferred into the diffracted wave in the case of Laue diffraction. This effect is associated with the interference of two pairs of coherent waves with $k_0^i(\varepsilon_1^i)$ and $k_0^i(\varepsilon_2^i)$, and also with $k_1^i(\varepsilon_1^i)$ and $k_1^i(\varepsilon_2^i)$, each travelling in its direction and differing in their wave vectors by a small amount. The resulting 'pendulum effect' (the spatially periodic conversion of the refracted wave into a diffracted wave and *vice versa*) can be observed only in a very thin layer of crystal, where absorption effects can legitimately be ignored and the amplitudes of all four waves have comparable magnitudes. Furthermore, in order to form a diffracted wave with a uniform cross-section the crystal must have a strictly constant thickness L_p over the whole aperture of the beam.

A wave field at the surface of the third crystal, identical with the first and oriented in the same way, can be obtained by noting that the rotation of two waves in space leads to the

replacement of $\boldsymbol{\kappa}$ by $\boldsymbol{\kappa}_1 = \boldsymbol{\kappa} + \boldsymbol{K}$ and $\boldsymbol{\kappa}_1 - \boldsymbol{K} = \boldsymbol{\kappa}$. The result is

$$E^i(r,t) = E_0^i(\varepsilon_1^i)\exp\left[\mathrm{i}(\omega t - \boldsymbol{\kappa}_1\cdot\boldsymbol{r} + \varphi_1)\right] + E_1^i(\varepsilon_1^i)\exp\left[\mathrm{i}(\omega t - \boldsymbol{\kappa}\cdot\boldsymbol{r} + \varphi_2)\right] . \quad (3.11)$$

We have allowed for the fact that during the propagation of two waves by different trajectories each wave can experience an additional phase change φ_1 and φ_2, owing to physical effects, and lying beyond the scope of the theory of diffraction. In keeping with the special features of the metrics and electrodynamics of rotating ring structures discussed above the parameters φ_1 and φ_2 in the modification of the Sagnac experiment being discussed are the result (in addition to possible fluctuation mechanisms) of the phase difference $\pm\varphi_0$ [Eqn (2.29)] associated with the motion of two waves in opposite directions in a rotating interferometer system. In order to generalise the discussion we shall assume that in addition to the phase shift $\pm\varphi_0$, each of the waves travelling in opposite directions can experience during its trajectory an additional phase change $\delta\varphi_{1,2}$, which allows a unified treatment of the insertion into the interferometer of corrective phase-shifting elements, and also of random fluctuations of the phases owing to the instability of the system parameters. Replacing the phases $\varphi_1 = \varphi_0 + \Delta\varphi_1$ and $\varphi_2 = -\varphi_0 + \Delta\varphi_2$ in Eqn (3.11) by their combinations $\varphi_{a,b} = (\varphi_1 \pm \varphi_2)/2$ gives

$$E^i(r,t) = \left\{[E_0^i + E_1^i\exp(\mathrm{i}\boldsymbol{K}\cdot\boldsymbol{r})]\cos\varphi_b + \mathrm{i}[E_0^i - E_1^i\exp(\mathrm{i}\boldsymbol{K}\cdot\boldsymbol{r})]\sin\varphi_b\right\} \times \exp\left[\mathrm{i}(\omega t - \boldsymbol{\kappa}_1\cdot\boldsymbol{r} + \varphi_a)\right] . \quad (3.12)$$

The last expression shows that because of the resulting phase shift φ_b the two coherent initial waves $E_{0,1}^i(\varepsilon_1^i)$, incident (symmetrically to the crystal planes with a doubled Bragg angle) on the surface of a third crystal mirror, form two coher-ent superpositions. Noting that the amplitudes of the inter-acting waves are related by Eqn (3.9) $E_1^i = -E_0^i = \varepsilon_0/2$, it is evident that for one of the superpositions (the first) the total field vanishes within the absorbing planes of the third crystal, which are an extension in space of the planes of the first crystal, whereas for the other superposition [the second in (3.12)] it reaches its maximum value in this region. As a result the first wave superposition (whose relative amplitude is $\cos\varphi_b$) passes through the third crystal, which plays the part of a phase analyser or a phase–amplitude converter without substantial absorption. After their passage through the crystal the two waves of this superposition are propagated along their independent trajectories and can be measured by amplitude detectors. At the same time a photographic plate located directly beyond the emergence surface of the third crystal can record the interference field of the waves.

The second wave superposition is strongly absorbed and decays very rapidly in the crystal: it is undetectable beyond it.

As a result of these processes the intensity of the radiation registered by each of the amplitude detectors located beyond the third crystal is given by $J \equiv J(\varphi_b) = (J_0/4)\cos^2(\varphi_b)$, where $J_0 = \tilde{E}_0^2\sigma_0 C/4\pi\hbar\omega$ is the intensity of the initial wave incident on the splitter crystal (first mirror) and σ_0 is the cross section of the beam.

In the modification of the Sagnac experiment which we are discussing the monocrystalline mirrors simultaneously solve the three problems which oppose the realisation of the experiment in the X-ray region: they act as the source of a pair of coherent X-ray waves (i.e. as the splitter), as very effective reflectors, and as a phase analyser. The counting rate of the quanta provides valuable information, corresponding to the angular rotation velocity Ω.

Let us examine the possibility of optimising the experiment. Because of the parabolic dependence of the velocity of light $N = J_t$ on Ω at low values of φ_b and Ω a significant increase in precision is possible by moving the working point φ_b ($\Omega = 0$) along the linear part of the amplitude–phase characteristic $J(\varphi_b)$. This can be achieved by inserting additional phase-shifting elements into one or both of the interferometer arms. If under these conditions $\Delta\varphi = (\Delta\varphi_1 - \Delta\varphi_2)/2 = \pi/4$ the $J(\varphi_b)$ dependence becomes

$$J = \frac{J_0}{8}\left[1 - \frac{4\pi S\Omega}{\lambda c}\right] . \quad (3.13)$$

There are several ways of introducing into the interferometer this additional 'linearising' shift ('phase substitution'). It can be done by placing phase plates in the apparatus or by additional rotation of the interferometer at a high angular velocity Ω_0, which offers the required value of $\Delta\varphi_1 - \Delta\varphi_2 = \pi/2$ at $\Omega_0 = \lambda C/8S$.

A more natural way of introducing the phase substitution is to use (as was suggested by experiments with an actual interferometer) the built-in field of small deformations, which leads to an equivalent additional phase shift $\Delta\varphi = \pi\Delta x/d$ as a result of the displacement of the crystal planes by Δx from their model position (the same for all three mirrors). Here d is the interplanar spacing.

In the case of a heterogeneous deformation field the quantity Δx is a smooth function of the coordinate x, perpendicular to the planes. For a relative deformation $\Delta d/d$ the overall interference field at the emergence surface of the last (third) mirror will be characterised by a moire pattern with period $\Lambda = d^2/\Delta d$. For a strong enough deformation the spatial period of this moire pattern can be comparable to the size of the trace of the incident X-ray beam $D = D_0/\cos\theta_0$, which requires allowing for the change in phase within the range of D. This is done by averaging the final expression for $J(\varphi_b)$ over the whole range of changes in $\Delta\varphi$ within the region $\delta\varphi = \pi D/\Lambda$. As a result we find

$$\langle J(\varphi_b)\rangle = \frac{J_0}{4}\frac{1}{\delta\varphi}\int_{\Delta\varphi-(\delta\varphi/2)}^{\Delta\varphi+(\delta\varphi/2)}\cos^2(\Delta\varphi + \varphi_0)\,\mathrm{d}(\Delta\varphi) = \frac{J_0}{8}\left[1 + F\cos 2(\Delta\varphi + \varphi_0)\right] , \quad (3.14)$$

where $F = \sin(\delta\varphi)/\delta\varphi$ is the aperture phase parameter of the beam.

This averaging produces a large decrease in the contrast of the structure of the interference field and lowers the precision of the measurement of angular velocity.

We shall now assess the prospects (in principle) of the Sagnac experiment carried out with X radiation. Ignoring the fluctuation processes in the interferometer system, which will be examined in detail below, we shall determine the dimensions of an interferometer able to measure the rate of rotation of the Earth. Tentatively assuming a maximum precision of the amplitude measurements of $\Delta N/N \approx 10^{-4}$ by the counting of quanta, we find from (3.13) that the smallest area of an interferometer able to determine the rate of rotation of the Earth by means of X radiation of wavelength $\lambda = 0.3$ A is $S_{\min} \approx 10$ cm^2.

With softer radiation and a smaller interferometer contour the effect of the rotation of the Earth on the gyroscopic effect is negligibly small. The experiment with the apparatus and radiation parameters $S \approx 4.28$ cm^2 and $\Lambda \approx 1.54$ A led to the same conclusion.

A further increase in the sensitivity of the Sagnac experiment can be produced by adopting a resonator scheme with a closed circular trajectory and multiple circuits.

The main problem met in the realisation of this scheme is the need to satisfy the requirements of a closed path for the motion of the quanta [22–29]. Without dwelling on this specific and complex problem we shall only mention some attempts to analyse its solution, including the use of a non-planar trajectory [22], the use of a figure-of-eight trajectory of the rays [23] (with cross-over), ultrasonic control of the Bragg diffraction parameters [24, 25], and asymmetric reflections [26]. The last of these models has already been realised, and used to construct the first (and so far, apparently, the only) working resonator in the X-ray band [27]. We shall not discuss the physical form of this resonator [28], but merely consider the maximum precision of the measurements of Ω of which the instrument is capable.

Consider the case when the characteristic frequency of one of the modes of the resonator coincides with the frequency of the radiation ω_0 applied from the source. When the system is rotating, the tuning frequency of the resonator is different for different directions [2, 30], and equal to $\omega_r = \omega_0(1 \pm 2S\Omega/lc)$.

Here l is the perimeter of the resonator. According to the theory of resonant systems, waves of identical frequency propagated in equivalent resonance circuits with different resonance frequencies acquire additional phase shifts $\varphi_0 = \pm \arctan(2Q\omega_0/\omega_0)$, where Q is the quality factor of the resonator.

For low values of $2Q\Delta\omega_0/\omega_0$ the difference in phase between waves travelling in opposite directions is

$$\varphi_0 = \pm \frac{4SQ\Omega}{lc} . \qquad (3.15)$$

When the appropriate 'phase substitution' is used to linearise the phase-amplitude characteristic of the counting rate of the quanta the increase in precision of the Sagnac experiment is determined by the ratio of the differences in phase for the resonator (3.15) and the interferometric scheme $\varphi_0 = \pm 2\pi S\Omega/\lambda c$, and is equal to $G = 2\lambda Q/\pi l$. The maximum value of Q (ignoring the diffraction losses, which are unimportant in the X-ray and gamma regions) is given by $Q^{\max} \approx 2\pi l/N_0\lambda(1-R)$, where R is the reflection coefficient for each of the N_0 mirrors of the resonator [10]. For this $Q^{\max}$ value we have $G^{\max} \approx 4/N_0(1-R)$.

Using the experimentally accessible value $R \approx 0.95$, and assuming $N = 4$, we obtain $G^{\max} \approx 20$. We note that in the case, which has already been realised and experimentally studied, of a germanium resonator the quality factor $Q \approx 2.6 \times 10^9$ determined experimentally [27] for a wavelength $\lambda \approx 1.8$ A corresponds to an almost three-fold increase in precision and sensitivity.

We should also note that the use of radiation whose spectrum occupies a frequency band $\delta\omega$ small in comparison with the intermode separation $\omega_1 = 2\pi c/l$ and with the transmission band of the resonator $\Delta\omega = \omega/Q$ is a necessary condition for the accumulation of phase shift during multiple circuits. For the already implemented and other possible single-block crystal resonators with parameters $Q > 10^9$, $\lambda \approx 10^{-8}$ cm, $l \approx 10$ cm we have $\omega_1 \approx 2 \times 10^{10}$ Hz and $\Delta\omega \leqslant 2 \times 10^{10}$ Hz, which is 4–5 orders of magnitude lower than the width of the characteristic X radiation band. Obviously, only the Mössbauer gamma radiation satisfies this necessary condition. The low activity of the isotopic Mössbauer gamma sources complicates the construction of resonator schemes for the Sagnac experiment.

4. Experimental assembly and possible error sources of the Sagnac experiment with X radiation

Because of the very high sensitivity of interference experiments using radiation with a short wavelength in the X-ray range towards weak perturbations (deformations of the crystal mirrors in a static position and during motion or under the influence of angular acceleration, temperature gradients, etc.) the experiment was planned to include several 'rigid' (ш-shaped) interferometers all made from a single silicon monocrystal by mechanical removal (cutting) of the unwanted parts followed by annealing, lapping, and chemical polishing. Additional rigidity was obtained by designing the single-block interferometers in the form of three thin mirrors connected by an upper and lower thick base fastened by four edge pillars (Fig. 4). The interferometer had external dimensions of 4.5 cm × 3 cm (measured along the perimeter of the reflecting mirrors), and was designed to use radiation from the characteristic Cu$K_{\alpha 1}$($\lambda = 1.541$ A) X-ray line in a system of (220) planes perpendicular to the mirror surfaces and having a period $d_{220} \approx 1.92$ A corresponding to the diffraction angle $\theta_0 \approx 23.65°$, and area of the contour $S \approx 4.28$ A cm^2. The length of each of the split trajectories was $l/2 \approx 6.4$ cm.

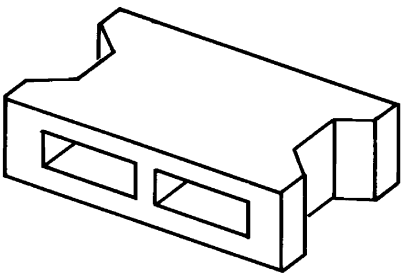

Figure 4. Single-block three-mirror crystal interferometer with corner rigidity pillars.

A preliminary study of the prepared interferometers confirmed the absence of moiré in the central region of the interference field (1 cm × 1 cm) on the emergence surface of the third mirror and a weak moiré (one band) on its periphery. This observation demonstrated the strict periodicity and the exact coincidence of the (220) planes in all three spaced-out mirrors.

A self-contained apparatus weighing 1500 kg and supported on a rotating platform was assembled in order to study the gyroscopic effect based on the Sagnac effect with X radiation. A large opening was provided at the centre of the platform to allow cooling water to be led to the X-ray tube and also to provide a three-phase power supply through slip-ring contacts (Fig. 5). The whole apparatus was rotated from

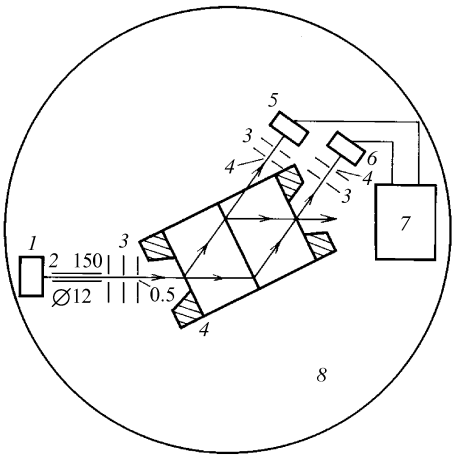

Figure 5. Arrangement of the Sagnac experiment on a rotating platform, using X radiation: (*1*) X-ray tube, (*2*) collimating tubulation, (*3*) diaphragms, (*4*) three-mirror crystal interferometer, (*5*) monitor counter, (*6*) main (signal) counter, (*7*) data processing system, (*8*) rotating platform. The sizes of the tubulation and of the horizontal and the vertical slits in the diaphragms are in millimetres.

a low-speed vibration-free (4A 112 MV 8UZ) electric motor through a gear-box.

An X-ray generator and tube (40 kV, tube current 30 mA), a 12 GUR-8 goniometer, and also a main counter and a monitoring counter, were placed on the rotating platform. The main counter was of the BDP 2-02 (proportional) type; the monitoring counter was a scintillation counter (type SRS-4-411). The system included electronic means of processing the signals from the counters. All the control units were duplicated on a nonrotating panel.

The monitoring counting channel was needed to eliminate the effects of the fluctuations in the power supply to the X-ray tube (i.e. of fluctuations in the intensity of the X radiation) on the results of measurements in the main channel. This was done by expressing the result obtained in all the possible measurement regimes (for a given time, for a given total number of pulses from the monitoring counter, or for a given number of complete rotations of the whole platform) as a ratio of the number of pulses from the main counter N to the number of pulses from the monitor counter N_M.

Serious difficulties arose in fixing the crystal interferometer rigidly on the platform of the rotating apparatus. All the attempts to attach the interferometer directly to the column of the goniometer head (direct location on a lapped surface or on a greased support, fixing the picein or plastilin wax, etc.) produced large deformations of the mirrors. As a result, because of the large and arbitrarily varying difference between the phases of the waves in different parts of the interferometer, the total field was strongly perturbed and was characterised on the topogram either by a moiré pattern with a small period or by a chaotic grain structure. One possible cause of this perturbation stems from the different values of the thermal expansion coefficient of the interferometer material, the fixing material, and the surface on which the interferometer is fixed. In the presence of the unavoidable instability of the temperature this state of affairs led to deformations and to a substantial perturbation of the final interference field [30]. The sensitivity of the structure of the interference field to deformations can be illustrated by quoting results similar to ours on the behaviour of a rotational moiré in a specially deformable three-mirror interferometer [31], according to which a rotation of one of the mirrors by 10^{-2} second of arc produces a moiré with a period of 4 mm.

The best method from the point of view of minimising the imposed deformations was found to be the 'soft' fixation of the interferometer by placing it on a soft cloth support attached to the stage of the goniometer head. However, this method of fixing produced inertia effects associated with the change in state of the system at the beginning and at the end of the rotation, and also after changes in the rate or in the direction of rotation of the platform. Preliminary experiments had shown that in all the changes in the state of the equilibrium rotation the interferometer was initially shifted (or rotation) in the direction of the inertia force and then slowly returned towards its final position (slightly different from the initial position). This relaxation took place over a period of several tens of seconds, which is incompatible with the need (pointed out below) to keep the measurement times short. The most suitable method of attaching the interfero-meter was found to be by providing four locating indentations under the pillars. With this modification the moiré pattern of the interference field was so large (3—5 mm) that a collimated X-ray beam could be oriented in the region of the local quasi-uniform field.

Another possible origin of uncontrolled deformations leading to a nonstationary perturbation of the final interference field is the temperature drift. By using a photographic method of multiple recording of the topograms of a given part of the interferometer it was possible to study the effect of temperature instability. The magnitude of this effect can be judged by the fact that changes in temperature of the surrounding medium of $\Delta T \approx 3-4$ K produce a change by 1 unit in the number of moiré bands in the interference pattern associated with the initial deformation.

Temperature drift effects were minimised by means of a thermal isolation system. The interferometer, made from sheets of foam plastic 4 mm thick in the shape of a rectangu-lar box, was placed in a thermally insulated chamber rigidly fixed to the goniometer head. In order to even out the temperature field the inner surface of the chamber was lined with copper plates 0.5 mm thick, and the outer surface with thermally reflecting aluminium foil.

The effectiveness of these modifications aimed at improving the thermal insulation and at eliminating uncontrolled nonstationary deformations by finding a suitable method of fixing the interferometer was tested during a study of the deviation of the experimental counting statistics for the signal channel from the Poisson statistics. A previous study had been made of the count rate statistics of the X-ray quanta in the monitor channel. The latter differed only very slightly from the Poisson statistics and was characterised by a root-mean-square error $[\langle (N_M - \bar{N}_M)^2 \rangle]^{1/2} \approx 1.76\sigma$ for $\bar{N}_M = 2.7 \times 10^6$ counts.

The counting statistics for the signal channel were then investigated by 10 successive measurements (counts) of the pulses in the signal channel N_{0i} with $i = 1, 2, \ldots, 10$ and a mean $\bar{N}_0(t)$ for a given count in the monitor channel N_{Mi} (circles). For the Poisson statistics the calculated root-mean-square error $\sigma(t)$ should correspond to the result of processing the experimental data if there are no additional (i.e. other than purely statistical) fluctuation mechanisms. The same method was applied in further studies of the

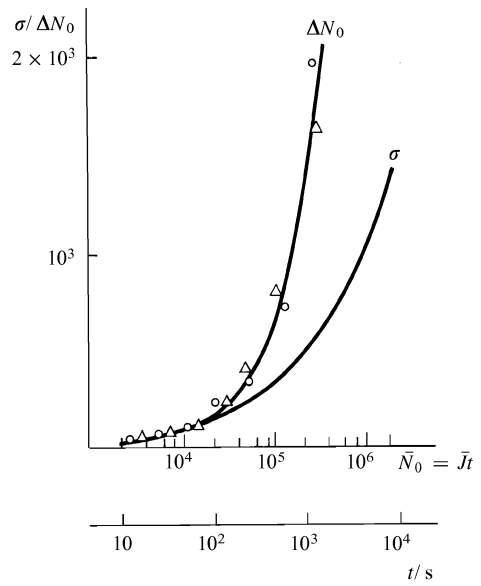

Figure 6. Experimental dependence of the root-mean-square counting error for the quanta $\Delta N_0(\bar{N}_0)$ and dispersion function of the Poisson statistics $\sigma(N_0)$ for the final interference field of the X radiation emerging from the interferometer.

counting statistics for fixed measurement times t (triangular signs) on the stabilised quartz generator.

The measurements by both methods were carried out over a wide range of measurement times (from 10 s to 2×10^3 s), and they showed (Fig. 6) that as a result of the suggested modifications the measurement statistics did not differ from the Poisson statistics for times up to $t = 70-80$ s, with most probable value of $t_0 = 73$ s. The latter time defines the upper limit of the reliable measurements in the signal channel, for which the effect of nonstatistical fluctuations is not significant. Without these improvements the reliable range of measurement times falls to a few seconds.

To determine the effectiveness of the action of the monitor channel separately we studied the effects of changes in the parameters of the operating regime of the X-ray tube on the results of the measurements of the N_{0i}/N_i ratio. Changes in the tube voltage from 30 to 40 kV or in the tube current from 30 to 25 mA produced very large changes in N_{0i} and N_{Mi}, but their ratio stayed the same.

Yet another possible source of measurement error could be the accelerometric effect, which is seen as a nonuniform deformation of different parts of the interferometer and as a different shift of the mirrors owing to the nonuniformity of the centrifugal acceleration and of the corresponding force $F = m\Omega^2 r$ during the rotation of the system. For small values of Ω and r, and also allowing for the rigid construction of the interferometer and for the well controlled orientation of the reflecting planes, this influence appears to be insignificant. It has also been studied in tests of the gyroscopic effect.

5. Experimental realisation of the Sagnac experiment with X radiation

Interference measurements of the angular velocity of rotation were carried out by placing the interferometer in a thermally insulated chamber and fixed to its base with picein wax at the corners of the rigidity pillars. The steel plinth carrying the X-ray tube, the goniometer with the interferometer, and the measurement counters were arranged so that the reflecting (220) atomic planes of the crystal mirrors were parallel to the radius of rotation and the central (second) crystal mirror was located exactly on the axis of the rotating platform with $r_1 = 0$. This choice of orientation for the (220) planes is necessary in order to avoid the accelerometric effect, since in this case the centrifugal deformation shifts the mirror only along the planes themselves and does not perturb the phase structure of the wave.

The vertical size of the beam was then substantially shortened, and the surface of the first mirror was scanned with a thin beam of X radiation while plotting the characteristics of the signal channel on a recorder chart. From the diagram thus obtained, which gave the intensity distribution $J(\Delta\varphi)$ (3.12), we took the initial phase difference $\Delta\varphi = \pi/4$ for an immobile platform, corresponding to the surface of the first mirror (which gave an emergent ray of intensity $J = J_{max}/2$ when the X-ray beam was focused on it). In the same way the working point with a maximum (linearised) steepness of the $J(\Omega)$ dependence (3.13) was chosen. After this the measurement was carried out [counting of the quanta $N = J(t)$] in this region of space while applying rotations in the right-hand (R) and in the left-hand direction (L). Occasional measurements (0) with $\Omega = 0$ were made at the same point as the control. The results of measurements for $\Omega = 0.45\ s^{-1}$ (rotation period of 14 s of the platform) are shown in Fig. 7 from data taken with a KSP-4 $x-y$ recorder. This series of (R, L, 0) measurements was repeated without interruption for several hours. During each measurement of N_R, N_L, N_0 (lasting up to 10 s, the complete series lasting approximately 30 s) the reproducibility of the results was very good. The average values $\bar{N}_R$, $\bar{N}_L$, $\bar{N}_0$ lie in an error band determined only by the laws of statistics. However, during each sequence of many series of measurements a change in $\bar{N}_R$, $\bar{N}_L$, $\bar{N}_0$ (usually an increase) was observed, though the differences $\bar{N}_R - \bar{N}_0$, $\bar{N}_0 - \bar{N}_L$ remained constant and equal to each other. This parallel shift of the whole picture was ascribed to thermal drift of the interference field structure.

The next step was the detailed quantitative study of the gyroscopic effect, using the monitor channel with allowance for the accelerometric effect.

Initially the interferometer was set up so that the distance from the axis of rotation to the second mirror was $r_2 = 5$ cm. Because of the small period of the moiré pattern of the inter-

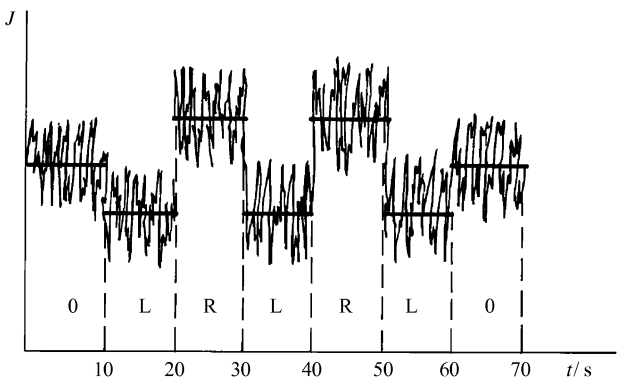

Figure 7. Dependence of the intensity of the X-ray interference field on the direction of rotation of the interferometer platform for an optimum initial difference in phase between waves moving in opposite directions: R denotes rotation towards the right, L towards the left.

ference field in the absence of rotation and of the relatively large size of the trace of the X-ray beam on the crystal the position of the working point (as was shown by subsequent studies) did not correspond to the optimum value $\Delta\varphi = \pi/4$. This did not affect the fixation of the gyroscopic effect.

Each series of measurements of the rotation effects consisted of three subseries, chosen sequentially for $\Omega_L = \Omega$, $\Omega_0 = 0$, and $\Omega_R = -R$. Each subseries consisted of 10 measurements. In each measurement the number of recorded pulses ($N_{R,L,0} \approx 3 \times 10^3$) was found for the given number of pulses in the monitoring channel $N_M = 4 \times 10^4$. This duration of each separate measurement allows the long-term temperature drift to be ignored.

An analogous series of measurements with an undetermined initial phase difference $\Delta\varphi$ was carried out for an initial displacement of the interferometer to the point $r_3 = 25$ cm.

The results of these measurements for all the 5 series and for the rotation of the platform bearing all the measurement apparatus at a frequency $\Omega \approx 0.6\ s^{-1}$ (rotation period $T = 10.4$ s) are shown in Fig. 8, together with data on the absolute root-mean-square errors for each subseries as well as for all the 5 series. A statistical treatment of the data showed that, as in the case of $r_2 = 5$ cm, even with $r_3 = 25$ cm the final error in the measurements on the whole complex 5 series satisfies the condition $\Delta N_{st} \approx \omega$, which confirms the absence of significant fluctuational error mechanisms other than the purely statistical mechanisms.

In the lower part of Fig. 8 we show the relative counting differences in different directions $(\bar{N}_R - \bar{N}_L)/\bar{N}_0$ for each series of measurements.

We suggest qualitative and quantitative interpretations of the measurement results. The very strong asymmetry in the counts N_R and N_L for the right and the left rotation directions respectively with respect to the state of rest (N_0) shows that

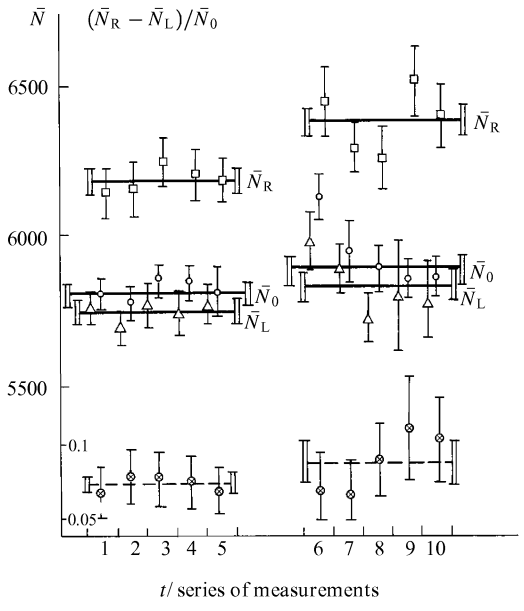

Figure 8. Number of counts of the quanta of the X-ray interference field during rotation of the platform towards the right (N_R) or towards the left (N_L), and for an immobile platform (N_0). Corresponding data for individual series of measurements are denoted by squares, triangles,or circles. The series 1–5 correspond to $r_2 = 5$ cm, the series 6–10 to $r_3 = 25$ cm. The circles with a cross describe $(\bar{N}_R - \bar{N}_L)/\bar{N}_0$.

the position of the working point did not correspond to the linear part of the phase characteristic, i.e. the experimental value $\Delta\varphi$ differed substantially from $\Delta\varphi_{opt} = (n \pm 1/4)\pi$.

The aperture–phase parameter F (3.14), allowing for the experimentally observed period of the moiré $\Lambda \approx 2.5$ mm and the width of the trace of the beam on the horizontal plane (the length of the intersection of the beam with the surface of the third mirror) $D \approx 0.55$ mm was $F \approx 0.92$.

By applying (3.14) to the case of three values of the angular velocity $\Omega_R = -\Omega$, $\Omega_0 = 0$, $\Omega_L = \Omega$ we obtain the system of equations

$$\frac{N_0}{N} = 1 + F\cos(2\Delta\varphi)\ ,$$
$$\frac{N_{R,L}}{N} = 1 + F\cos[2(\Delta\varphi \pm \varphi_0)]\ ,$$
$$N = \tfrac{1}{8}J_0 t\ , \qquad (5.1)$$

which relates the required parameters of the angular rotation velocity and of the phase of the working point with the values of the relative number of counts in these three regimes. This system is easily converted into

$$[1 + F\cos(2\Delta\varphi)\cos(2\varphi_0)][1 + F\cos(2\Delta\varphi)]^{-1} = (N_R + N_L)(2N_0)^{-1}\ , \qquad (5.2)$$
$$F\sin(2\Delta\varphi)\sin(2\varphi_0)[1 + F\cos(2\Delta\varphi)]^{-1} = (N_R - N_L)(2N_0)^{-1}\ ,$$

even for $F < 1$, and for low rotation rates ($2\varphi_0 \ll 1$) we have

$$2\varphi_0 \cong \left\{\frac{1-F}{F}\left[\frac{N_R + N_L - 2N_0}{N_0} + \left(\frac{N_R - N_L}{N_0}\right)^2 \frac{1}{2F}\right]\right\}^{1/2},$$
$$\tan(2\Delta\varphi) \cong -\varphi_0(N_R - N_L)(N_R + N_L - 2N_0)^{-1}\ . \qquad (5.2a)$$

Let us first consider the results of measurements with $r_2 = 5$ cm:

$$(\bar{N}_R - \bar{N}_L) \approx 0.69(\bar{N}_R + \bar{N}_L - 2\bar{N}_0)\ . \qquad (5.3)$$

By using the measurement results for $(\bar{N}_R + \bar{N}_L - 2\bar{N}_0) \approx 5.15 \times 10^{-2}\,\bar{N}_0$ we find the required difference in phase between the waves travelling in opposite directions $2\varphi_O \approx 0.064 \pm 0.012$, associated with rotation. Under these conditions the final phase of the working point differed from $(n \pm 1.2)\pi$ by ± 0.022.

Similarly, for $r_3 = 25$ cm $(\bar{N}_R + \bar{N}_L - 2\bar{N}_0) \approx 7.11 \times 10^{-2}\,\bar{N}_0$, and $(\bar{N}_R - \bar{N}_L)/(\bar{N}_r - \bar{N}_L - 2\bar{N}_0) \approx 1.33$. In this case $2\varphi_0 \approx 0.075 \pm 0.014$. In this position of the interferometer the difference between the phase of the working point $\Delta\varphi$ and the same value of $(n \pm 1/2)\pi$ was ± 0.022.

It can be seen that the final position of the working point for two successive positions of the interferometer was far from the optimum value $(n \pm 1/4)\pi$ and close to the least favourable value $(n \pm 1/2)\pi$. Nevertheless there was no obstacle to the observation of the Sagnac effect.

Allowing for the relationship between $|\varphi_0| = 2\pi S(\Omega/\lambda c)$ and the angular velocity of the rotation Ω for given values of the parameters S and λ we finally obtain expressions for the measured value $\Omega \approx (0.55 \pm 0.1)\ s^{-1}$ for $r_2 = 5$ cm and $\Omega \approx (0.64 \pm 0.12)\ s^{-1}$ for $r_3 = 25$ cm, which agrees well with the accurate value found in practice for the rotating platform $\Omega = 0.604\ s^{-1}$. The agreement (allowing for the

statistical error band) between the experimental values of the angular velocity for the coordinates r_2 and r_3 of the centre of the interferometer shows that this behaviour is due to the gyro-scope effect and not to a deformation (accelerometric) effect.

6. Conclusions

The quantitative agreement between the results of the theoretical analysis of the electrodynamic process taking place in the X-ray band in a rotating crystal interferometer system and the experimental results suggests that the Sagnac effect can be reliably observed in X radiation.

Some very serious but purely technological difficulties (including the effects of thermal instability and of the deformation of the interferometer blocks) have prevented the achievement (in the first realisation of the Sagnac experiment in the X-ray band) of all the potential advantages offered by the use of shorter wavelengths on going from the optics of the visible region to those of the X-ray region.

A substantial improvement in the precision of the characteristics of the experiment can be achieved by adopting a resonator scheme involving a single pass of the X-ray beams along coincident trajectories. The resulting mutual compensation of the fluctuation interactions allows the theoretical precision limits of the measurement to be realised: these limits are set (at least in principle) by the counting statistics only. This optimisation makes possibly not only a test of the Sagnac effect (which originates from a change in the metrics of rotating systems without a material medium) but also a test of the weak effect of the rotation on the characteristics of the medium itself (in particular, the susceptibility and its anomalously strong dependence on the parameters of the nonrelativistic motion). In the optics of the visible range the effect of rotation on the electrodynamics of material media can be studied by alternative methods: the 'passive' Sagnac experiment and the 'active' laser gyroscope. In the X-ray range, because of the very serious difficulties met in the construction of X-ray and of gamma lasers [28], there are no alternative Sagnac experiments. We expect the current interest in this experiment to continue until the end of the century [2, 3, 32–34].

References

1. Michelson A *Phil. Mag.* **8** 716 (1904)
2. Sagnac G *C R. Ac. Sci.* (*Paris*) **157** 708 1410 (1913)
3. Sagnac G *J. de Phys. Ser.* 5.4 177 (1914)
4. Michelson A, Gale H *Astrophys. J.* **61** 140 (1925)
5. Michelson A, Gale H *Nature* (*London*) **115** 566 (1925)
6. Berstein A *Dokl. Akad. Nauk SSSR* **75** 635 (1950)
7. Okosy T, Okamoto K *Fiber-Optical Sensors* [Translated into Russian; Leningrad: Energoatomizdat, 1990]
8. Werner S A, Standenman J L *Phys. Rev. Lett.* **43** 1103 (1979)
9. Vysotskii V I, Vorontsov V I *Relativistskaya Astrofizika, Kosmologiya, Gravitatsionnyi Eksperiment* (Relativistic Astrophysics, Cosmology, Gravitational Experiment) (Minsk: Izd. Akad. Nauk BSSR, 1975) p. 130–131
10. Vysotskii V I, Vorontsov V I, Mazur A E, Preprint, Institute of Physics of the Ukrainian Academy of Sciences, No. 12 (Kiev, 1982)
11. Bezirganyan P A, Preprint, Erevan State University, FTT-3 (Erevan University, 1981)
12. Vysotskii V I, Vorontsov V I, Kuzmin R N, in *Doklady Vsesoyuznogo Soveshchaniya po Ispol'zovaniyu Sinkhrotronnogo Izlucheniya. SI-82* (Reports of the All-Union Conference on the Application of the Synchrotron Radiation. SI-82) (Novosibirsk: Siberian Branch of the Academy of Sciences of the USSR, 1982) p 150–155
13. Fedorov B F, Sheremet'ev A G, Umnikov V N *Opticheskii Kvantovyi Giroskop* (The Optical Quantum Gyroscope) (Moscow: Mashinostroenie, 1973)
14. Tonnelat M A *The Basis of Electromagnetism and Relativity Theory* [Translated into Russian; Moscow: Inostr. Lit., 1962)]
15. Levashov A E *Dvizhenie i Dvoistvennost' v Relativistskoi Elektrodinamike* (Motion and Duality in Relativistic Electrodynamics) (Minsk: Belarussian State University Press, 1979)
16. Landau L D, Lifshitz E M *Teoriya Polya* (Moscow: Nauka, 1988) [English translation: *The Classical Theory of Fields* (Oxford: Pergamon Press, 1983)]
17. Vorontsov V I *Nevzaimnye Yavleniya v Elektrodinamike Dvizhushchikhsya Sistem* (Independent Phenomena in the Electrodynamics of Moving Systems) (Kiev: Kiev State University Press, 1984)
18. Afanas'ev A M, Kagan Yu M *Zh. Eksp. Teor. Fiz.* **48** 327 (1965) [*Sov. Phys. JETP* **21** 17 (1965)]
19. Vysotskii V I, Vorontsov V I *Fiz. Tverd. Tela* **17** 2044 (1975)
20. Belyakov V A *Usp. Fiz. Nauk* **115** 553 (1975) [*Sov. Phys.-Usp.* **18** 267 (1975)]
21. Borrmann G *Zs. Phys.* **42** 157 (1941)
22. Bond W L, Duguay M A, Rentzepis P M *Appl. Phys. Lett.* **10** 216 (1967)
23. Cotterill R M *Appl. Phys. Lett.* **12** 403 (1968)
24. Vorontsov V I, Vysotskii V I, in *Kvantovaya Elektronika* (Quantum Electronics) (Kiev: Naukova Dumka, 1974) No. 8, p. 63
25. Vysotskii V I, Vorontsov V I, in *Prikladnaya Yadernaya Spektroskopiya* (Applied Nuclear Spectroscopy) (Moscow: Atomizdat, 1976) No. 6, p. 142.
26. Rostomyan A H, Bezirganyan P H *Acta Crystallogr. A* **34** 240 (1978)
27. Rostomyan A H *Rentgenovskie Rezonatory* (X-ray Resonators) Author's Summary of Ph. D. Thesis in phys.-math. sciences (Ashtarak Engineering-Physics Institute, Academy of Sciences of the Armenian SSR, 1980)
28. Vysotskii V I, Kuzmin R N *Gamma-lazery* (Gamma-Lasers) (Moscow: Moscow State University Press, 1989)
29. Kolpakov A V, Kuzmin R N, Ryabov V M *J. Appl. Phys.* **41** 3549 (1970)
30. Pinsker Z G *Rentgenovskaya Kristallooptika* (X-ray Crystal Optics) (Moscow: Nauka, 1982)
31. Bonze U, Hart M *Appl. Phys. Lett.* **6** 155 (1965)
32. Vavilov S I *Eksperimental'nye Osnovaniya Teorii Otnositel'nosti* (Experimental Foundation of Relativity Theory) (Moscow, 1928)
33. Sommerfeld A *Optics* (New York: Academic Press, 1954)
34. Tonnelat M A *Les Verifications Experimentales de la Relativite Generale* (Paris, 1984)
35. Logunov A A, Chugreev Yu V *Usp. Fiz. Nauk* **156** 138 (1888) [*Sov. Phys.-Usp.* **31** 861 (1988)]